Nano Energy 58 (2019) 596–603

Contents lists available at ScienceDirect

Nano Energy

journal homepage: www.elsevier.com/locate/nanoen

Communication

Controlled synthesis and room-temperature pyroelectricity of $CuInP_2S_6$ ultrathin flakes

Lin Niu[a,1], Fucai Liu[a,c,1], Qingsheng Zeng[a,1], Xiaoyang Zhu[b], Yanlong Wang[d,g], Peng Yu[a], Jia Shi[b], Junhao Lin[e], Jiadong Zhou[a], Qundong Fu[a], Wu Zhou[f], Ting Yu[d], Xinfeng Liu[b,*], Zheng Liu[a,h,*]

[a] School of Materials Science & Engineering, Nanyang Technological University, Singapore 639798, Singapore
[b] CAS Key Laboratory of Standardization and Measurement for Nanotechnology, CAS; Center for Excellence in Nanoscience, National Center for Nanoscience and Technology, Beijing 100190, China
[c] School of Optoelectronic Science and Engineering, University of Electronic Science and Technology of China, Chengdu 610054, China
[d] Division of Physics and Applied Physics, School of Physical and Mathematical Sciences, Nanyang Technological University, Singapore 637371, Singapore
[e] Department of Physics, Southern University of Science and Technology, Shenzhen 518055, China
[f] School of Physical Sciences and CAS Key Laboratory of Vacuum Sciences, University of Chinese Academy of Sciences, Beijing 100049, China
[g] Key Laboratory of Chemical Lasers, Dalian Institute of Chemical Physics, Chinese Academy of Sciences, Dalian 116023, China
[h] Environmental Chemistry and Materials Centre, Nanyang Environment & Water Research Institute, 1 Cleantech Loop, Singapore 637141, Singapore

ARTICLE INFO

Keywords:
2D pyroelectric materials
Controlled synthesis
vdW device
Temperature-dependent property
Pyroelectric nanogenerator
Ferroelectric materials

ABSTRACT

Since the very recent discovery of ferroic ordering under two dimensional limit, novel devices based on 2D ferroelectricity or ferromagnetism has attracted a lot of interests and are promising for next generation electronic and optoelectronic applications. We find that, below the transition temperature T_c ~320 K, ultrathin $CuInP_2S_6$ (CIPS) nanoflakes down to bilayer are still pyroelectric. Changing the temperature will lead to charge modification at the surface of CIPS. 2D pyroelectric nanogenerator is fabricated which can efficiently convert the pyroelectric charges into electrical current. This work will facilitate novel applications of pyroelectric and ferroelectric materials, including pyroelectric devices, thermal sensors, ultrathin nanogenerators and various van der Waals (vdW) heterostructure at room temperature.

1. Introduction

Ferroelectric materials exhibit spontaneous electric polarization due to the separation of the positive and negative charges at both sides of the crystal's surface. Below T_c, ferroelectric materials can be polarized by heating or cooling, and electrical charges will be generated at both sides of the crystals [1–9]. Therefore, ferroelectric materials are naturally pyroelectric.[10] Hundreds of pyroelectric and ferroelectric materials have been discovered for the fabrication of electronic and optoelectronic devices [1–3,11–21]. However, the three-dimensional nature of extensively studied ferroelectric oxide lattices limits the growth of high-quality ferroelectric films and heterostructure. Pyroelectric devices at the nanometer or atomic scale is still under exploration. Recently, two-dimensional (2D) metal phosphorus quadrichalcogenide crystals (MPDs, $A^IB^{II}P_2S_6$ and $A^IC^{III}P_2S_6$, in which A^I = Ag or Cu, B^{II} = Mn, Cd or Zn, and C^{III} = V, Cr or In) [22–27] have been revisited and serve as an excellent platform to explore the ferroelectricity in the limit of few-atom-thickness. They are van der Waals (vdW) ferroelectric crystals with low surface energy and could be deposited into 2D nanoflakes simply by mechanical exfoliation. Among them, room-temperature ferroelectricity of 2D $CuInP_2S_6$ (CIPS) has been reported with a ferroelectric-paraelectric transition temperature of T_c ~320 K [28–30]. In our previous studies, we have explored the switchable polarization in ultrathin nanoflake (4 nm) and demonstrated non-volatile memory devices by using a CIPS/Si ferroelectric heterostructure [28]. The atomically thin CIPS provide an interesting platform for the investigations of pyroelectric phenomenon, including in-situ pyroelectric surface/interface, pyroelectric process, and the pyroelectric current at the 2D limits.

In this work, by well controlling the appropriate growth time and temperature, we synthesize high-quality CIPS single crystals by using solid state reaction. Raman spectra reveals that the evolutions of Raman peaks are sensitive to the temperature, which are contributed to the change of polar order and ionic conductivity of CIPS induced by varying the temperature. Kelvin probe force microscopy (KPFM) as an in-situ measurement quantitatively provides information on surface

* Corresponding authors.
E-mail addresses: Liuxf@nanoctr.cn (X. Liu), Z.Liu@ntu.edu.sg (Z. Liu).
[1] These authors contributed equally to this work.

https://doi.org/10.1016/j.nanoen.2019.01.085
Received 18 December 2018; Received in revised form 21 January 2019; Accepted 30 January 2019
Available online 31 January 2019

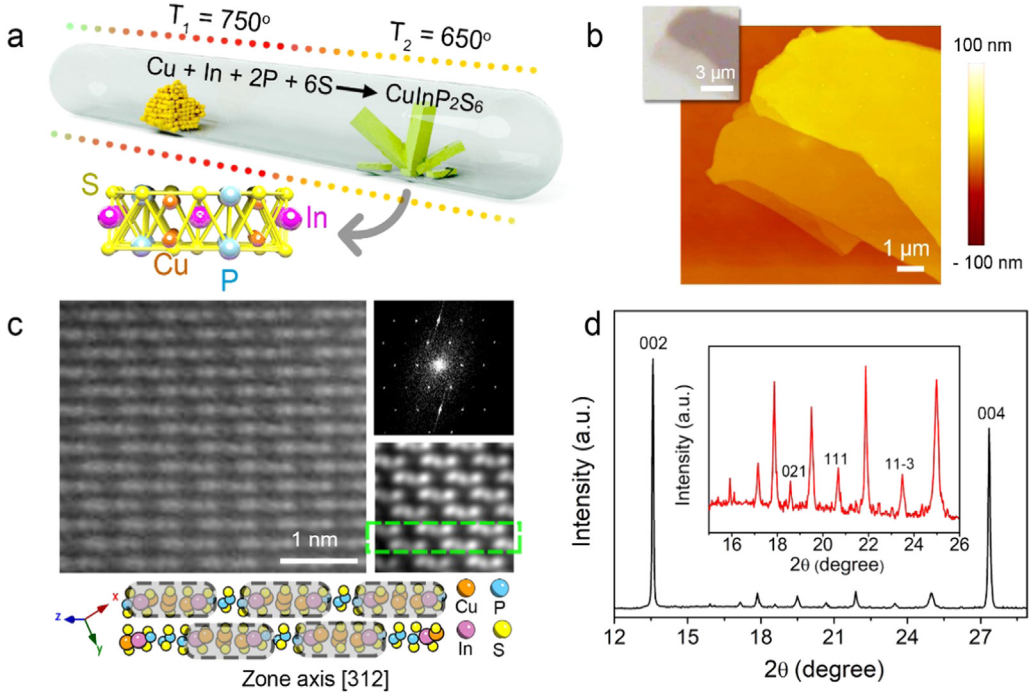

Fig. 1. Overall morphologies of the CIPS nanoflakes on silicon substrate. (a) Single crystals of CIPS were grown by the method of chemical vapor transport (CVT). (b) The morphologies of CIPS nanoflakes with different thicknesses were examined by optical microscopy and AFM. (**c**) STEM characterizations of CIPS crystal along the [312] zone axis, including the Z-contrast STEM image, corresponding fast Fourier transform (FFT) pattern and projected atomic model. In the atomic model, the yellow networks are S triangular networks, and the orange, purple and blue balls are Cu, In and P atoms, respectively. (d) X-ray diffraction patterns of CIPS crystal on Si/SiO_2 substrates with the ferroelectric phase (space group C_c at $T < T_c$).

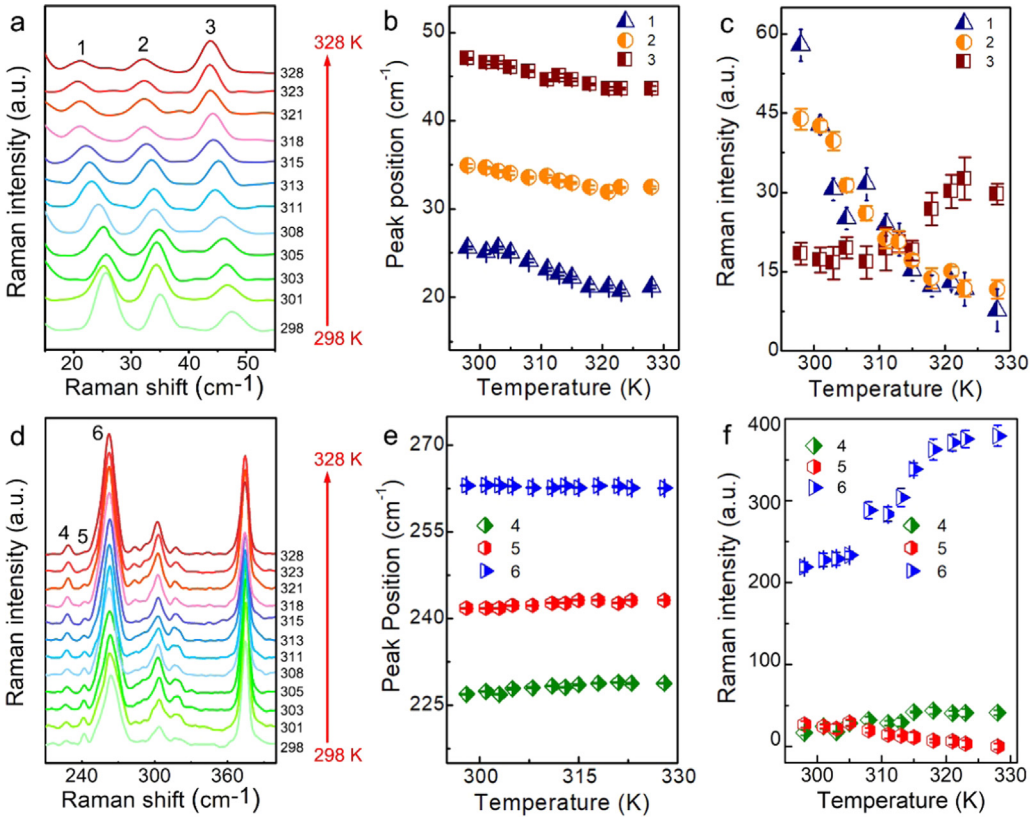

Fig. 2. Raman spectra of the CIPS nanoflakes and evolution of Raman signatures with temperature increase. (a) Raman spectra of the CIPS nanoflakes in the low-energy range with different temperature from 298 K to 328 K. In the measured spectral range of 10–60 cm^{-1}, the Raman spectra reveal three distinct bands at (1) 26, (2) 35, and (3) 47 cm^{-1} assigned to the cation translation modes. (b-c) Peak position and intensity evolution for bands 1–3 with the temperature increase. (d) Raman spectra of the CIPS nanoflakes in the higher-frequency range with different temperature from 298 K to 328 K. In the measured spectral range of 200–300 cm^{-1}, the Raman spectra reveal three distinct bands at (4) 220, (5) 240, and (6) 270 cm^{-1} assigned to the anion deformation modes. (e-f) Peak position and intensity evolution for band 4–6 with the temperature increase. The excitation wavelength used for Raman measurements is 532 nm.

topography and temperature-dependent surface potential modification simultaneously, characterizing the pyroelectric charges on the surface of CIPS nanoflakes at nanoscale. Further studies reveal that these pyroelectric charges could be harvested and converted into pyroelectric currents, realizing CIPS based vdW nanogenerator.

2. Experimental section

2.1. Sample preparation

High-quality CIPS single crystals were synthesized by solid state reaction as previously reported [31]. Ultrathin CIPS flakes were obtained by mechanical exfoliation from synthetic bulk CIPS crystals onto heavily doped silicon (Si) substrates.

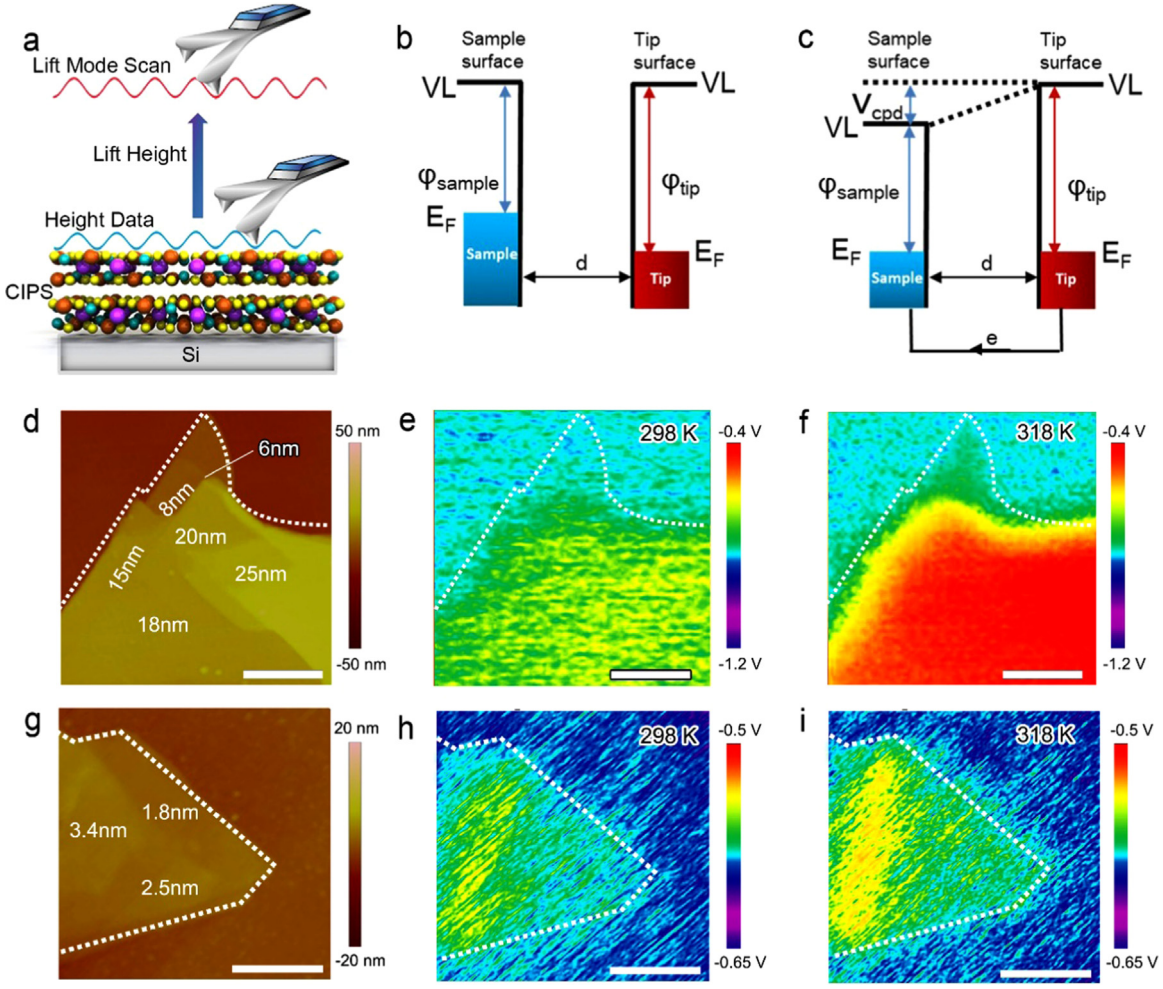

Fig. 3. Surface potential investigation for CIPS flakes with different thickness. (a) Schematic illustration of KPFM work mechanism. Band diagram of tip and sample when they are electrically separated (b) or electrically contacted (c). VL is the vacuum energy level. φ_{sample} and φ_{tip} are Fermi energy levels of the sample and tip, respectively. V_{CPD} is the contact potential difference. (d) AFM topography for CIPS flakes ranging from 6 to 25 nm thick, on doped Si substrate. (e) Corresponding potential mapping at 298 K. (f) Potential mapping changing by the heating from 298 K to 318 K. AFM topography (g), potential mapping at 298 K (h) and temperature-dependent change of potential mapping (i) of 1.8–3.4 nm thick (2–4 layer) CIPS on doped Si substrate. The scale bar is 1 μm.

2.2. Characterization of CIPS nanoflakes

Thickness of the flakes was identified from their optical contrast and AFM. PFM measurement was carried out by using an Asylum atomic force microscope (Asylum Research MFP-3D). The CIPS samples for transmission electron microscope (TEM) were prepared by dropping the solution with exfoliated CIPS thin flakes onto lacy carbon TEM grids. Z-contrast STEM imaging was done with a Nion UltraSTEM-100, operated at 60 kV, equipped with a fifth order aberration corrector. The convergence angle is set to be ~30 mrad. All Z-contrast STEM images were acquired from the ~86–200 mrad range. Raman spectra were carried out using a confocal Raman system (WITec) with the 532 nm laser excitation. X-ray diffraction patterns (2θ scans) were obtained from CIPS nanoflakes on the SiO2/Si substrates using an X-ray diffractometer (XRD Shimadzu Thin Film), using Cu-Kα radiation (λ = 1.54050 Å) within a diffraction angle (2θ) from 5° to 30°.

2.3. KPFM measurement

The KPFM measurements were performed using Bruker Dimension Icon Scanning Probe Microscopy with Nanoscope V controller. All the KPFM images were collected in lift mode by using SCM-PIT probes (Pt/Ir coated probes) with a spring constant of ~3 N/m and a resonant frequency of ~75 kHz. During all KPFM measurements, the optimal lift height is 50 nm (the details in Supporting Information, Fig. S7). Heating process was carried out by using TAC thermal applications controller.

2.4. CIPS device fabrication and measurement

The CIPS devices were fabricated by exfoliating the thin flakes of CIPS onto heavily doped silicon substrates. The top electrodes are defined using standard photolithography process followed by thermal evaporation of the Ti/Au (1 nm/10 nm) metal, and lift-off process. Thickness and size of the CIPS flakes and the Ti/Au electrodes were identified from their optical contrast and AFM.

2.5. Peakforce TUNA measurement

All the pyroelectric current measurements of CIPS nanoflakes were performed using Bruker Peakforce TUNA modulus. All the current images and curves were collected in contact mode by using SCM-PIT probes.

3. Results and discussion

We prepared the single crystals CIPS by chemical vapor transport (CVT) method as shown in Fig. 1a. Mixture elements of Cu, In, P, and S in stoichiometric proportion 1:1:2:6 were mixed as precursors. The air-

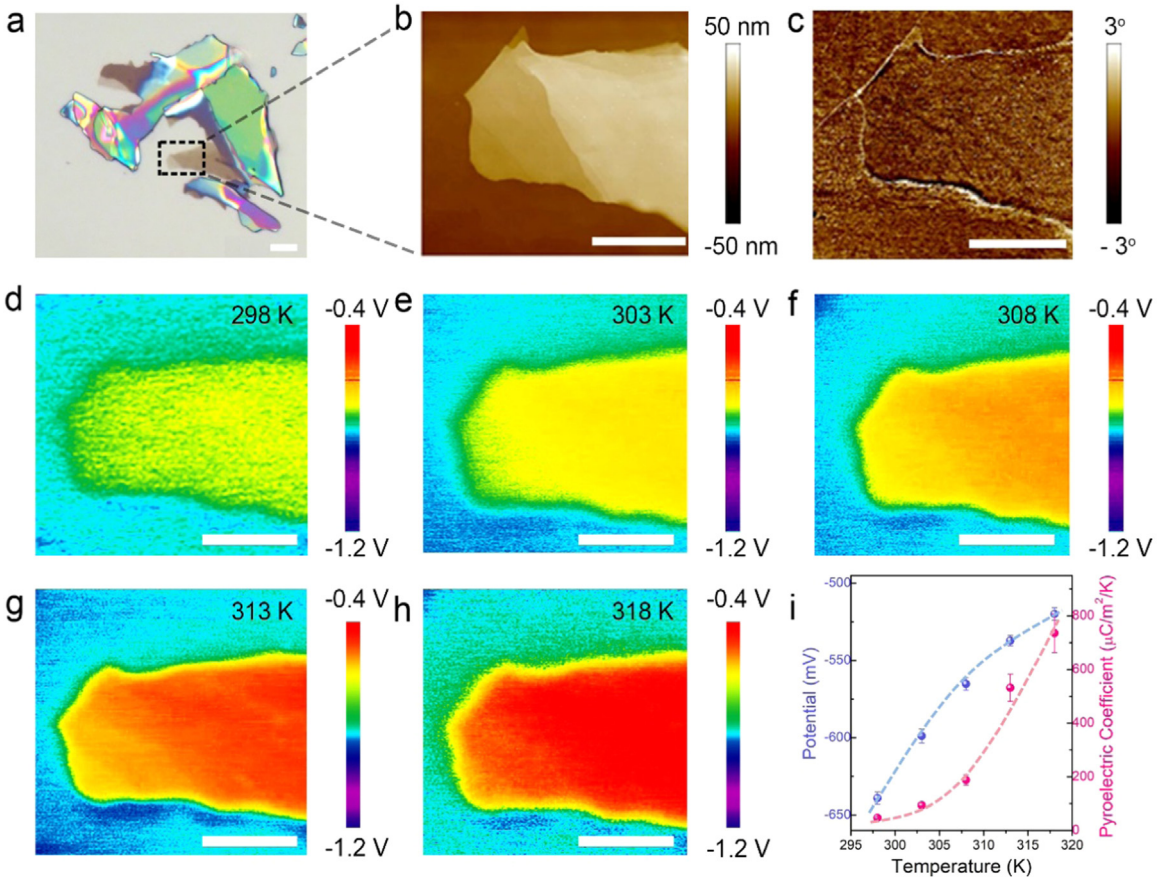

Fig. 4. Surface potential investigations for CIPS nanoflakes with different temperature. AFM topography (b) and phase (c) images observed by KPFM mode for the CIPS flake in a. (d–h) Corresponding potential mappings with the temperature of 298 K, 303 K, 308 K, 313 K and 318 K, respectively. (i) Average potential variations versus applied temperature calculated from (d–h). Error bars indicate one standard deviation. The scale bar is 2 μm.

stable yellow sample in the form of platelets can be collected in 2 weeks from evacuated silica tubes. Ultrathin CIPS nanoflakes with different thicknesses from 1 to 2 nm to hundreds were mechanically exfoliated on heavily doped Si substrate. They can be identified by color contrast in an optical microscope as shown in the inset of Fig. 1b and Fig. S1. The morphologies and thicknesses of the nanoflakes were identified by atomic force microscopy (AFM) height profiles as shown in Fig. 1b. The atomic structure and quality of the CIPS crystal were further confirmed by atom-resolved scanning transmission electron microscope (STEM) in Fig. 1c and Fig. 2, with the corresponding fast Fourier transform (FFT) patterns and atomic models along the zone axis [312] and [316]. From the STEM image, the metal cations (Cu, In) and P-P occupy the octahedral voids of a sulfur framework. Cu, In and P-P pairs arrange in the triangular motifs and two adjacent monolayers form a complete unit cell because of the alternate site between Cu and P-P pair from one layer to the neighboring one (the bottom part in Fig. 1c). The CIPS is also characterized by using X-ray diffraction patterns (XRD). A set of strong peaks at 13.58 and 27.34 were assigned to [002] and [004] and another set of weak peaks at 18.57, 20.67, and 23.48 were assigned to [021, 111], [11-3] of the $CuInP_2S_6$ crystal (ferrielectric phase, space group C_c at $T < T_c$) with polar Cu sublattice as shown in Fig. 1d [32].

When $T < T_c \approx 320$ K, CIPS is pyroelectric (by heating or cooling) with polar Cu^I and In^{III} sublattices shifting in antiparallel directions relative to the midplane, and exhibits reversible spontaneous polarizations [24,31–33]. From the Raman spectra of CIPS, major signals are observed at two regions below 400 cm^{-1}, one at $10 < \omega < 60$ cm^{-1} and the other at $200 < \omega < 300$ cm^{-1}, as shown in Fig. 2 and Fig. S3. In the low-energy range, we observe clear signals of Raman peaks at 26, 35, and 47 cm^{-1} from Fig. 2a, which can be assigned to the CIPS cation translation modes [33]. Interestingly, the positions of all three peaks show temperature dependence: anomalous decreases for the wavenumbers of 26–21 cm^{-1}, 35–32 cm^{-1} and 47–44 cm^{-1} (red shift) are observed in the heating process at $T < T_c$ as shown in Fig. 2b. These three peaks are labelled as 1, 2 and 3 in Fig. 2a–c. Moreover, Raman intensities of the spectral lines in Fig. 2c demonstrate that these three low-energy bands appear obvious intensity redistribution with the temperature increase. These low-energy Raman evolutions can be attributed to the copper cation translations. Heating the CIPS nanoflakes leads to copper hopping motions between its twofold equivalent and the off-center intralayer site and the loss of polarity until CIPS transfers into the paraelectric nonpolar phase [25]. Meanwhile, we can find the Raman peaks in the higher-frequency range, assigning to the P_2S_6 anion deformation modes [33]. Three mainly three peaks at 220, 240 and 270 cm^{-1} can be found and they are labelled as 4, 5 and 6 in Figs. 2d–2f. These peaks can be ascribed to the P_2S_6 deformation variations, including P-P pair off-centering, PS_3 group twists, P-S distance and S-P-S angle changes. Apparently, there are blue-shifts for the position of peak 4 and 5 by increasing the temperature from 298 K to 328 K and a slight red-shift for peak 6: 226–229 (blue shift), 241–243 (blue shift) and 263–262 (red shift). Meantime, obviously intensity increase can be seen for peak 6. These observations correspond to the occurrence of a first-order phase transition in CIPS crystal between 298 K and 328 K. Greater copper content leads to an intensity increase for the band at 226 cm^{-1} and 263 cm^{-1} and a decrease for the band at 241 cm^{-1}. Therefore, all of the anion deformation modes are closely related to distortions within the sulfur framework occupied by Cu^I. These sensitive temperature-dependent evolutions of Raman peaks are originated from the slightly change of the atom positions within the

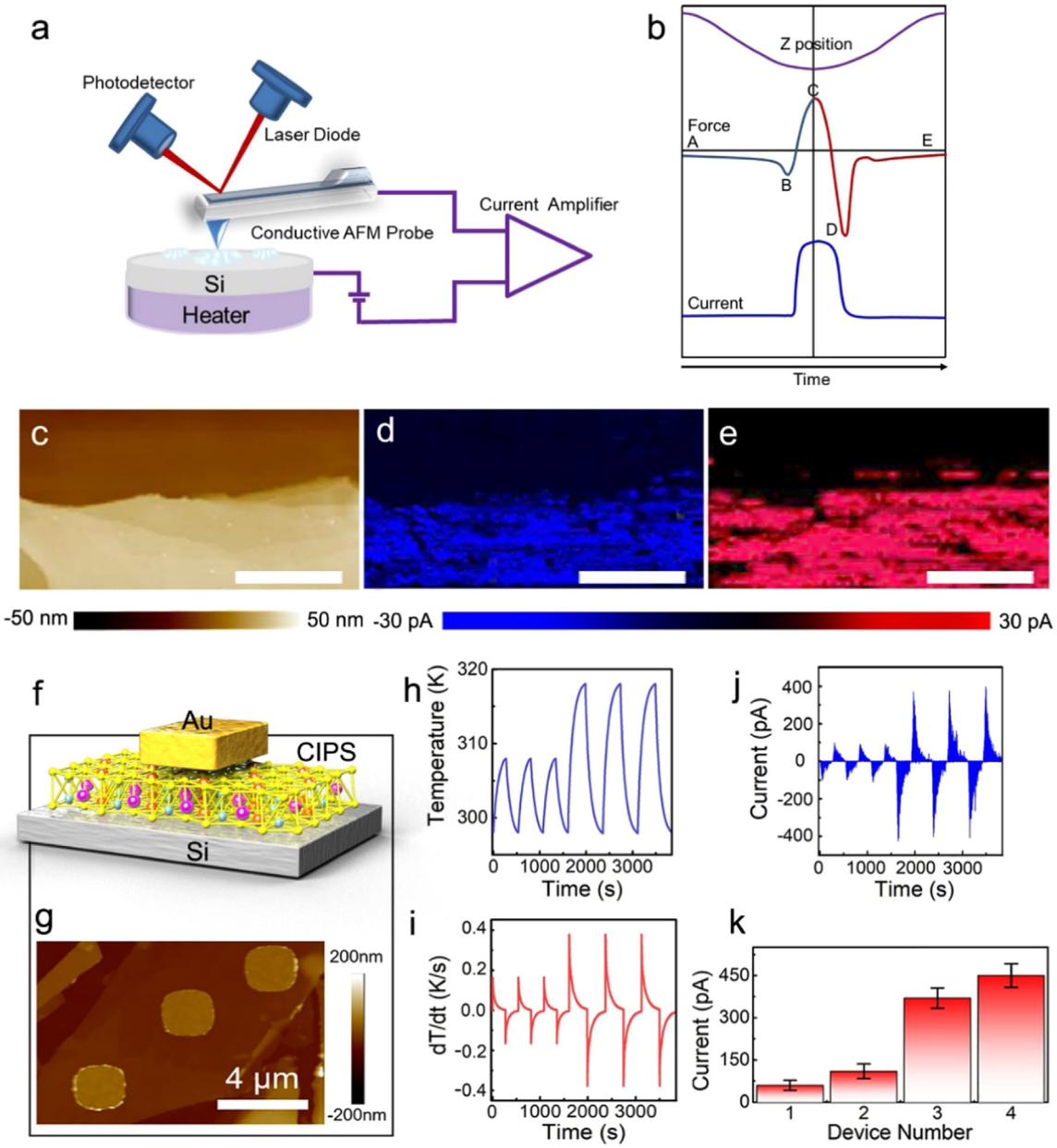

Fig. 5. Pyroelectric devices of CIPS nanoflakes. (a) Illustration of PeakForce TUNA setup for simultaneous topography and electrical property mapping. (b) Plots of Z position, Force, and Current as a function of time during one PeakForce Tapping cycle, with critical points including (B) jump-to-contact, (C) peak force, (D) adhesion labelled. AFM topography (c), TUNA current map (heating from 298 K to 318 K) (d) and TUNA current map (cooling from 318 K to 298 K) (e) of CIPS flake is observed by PeakForce TUNA mode. The scale bar in (c-e) is 2 μm. (f) Schematic and (g) AFM image of the vdW CIPS/Si device with 20 nm thick CIPS. (h) The cyclic changes in temperature (298 K–318 K–298 K and 303 K-308 K–303 K), (i) the corresponding differential rate curve, (j) the measured output TUNA current of the vdW CIPS/Si devices as pyroelectric devices under the temperature changes and (**k**) the TUNA currents with different electrode sizes are observed by using PeakForce TUNA mode.

CIPS crystal and therefore regulate the polarity of Cu, In and P_2S_6 sublattices and the CIPS intrinsic ion potential.

The changes of the CIPS intrinsic ion potential and charge displacement will regulate the pyroelectric charges on the CIPS surfaces. In order to characterize the charges quantitatively in real-time, the pyroelectric process of ultrathin CIPS nanoflakes is investigated by using Kelvin probe force microscope (KPFM) with lift mode as shown in Fig. 3a [34–37]. Figs. 3b and 3c illustrates the band diagram changes of the sample and tip in KPFM mode. A contact potential difference V_{CPD} could be explored based on the electrically contacted and work function differences between the sample (φ_{sample}) and the tip (φ_{tip}). Therefore, we could track V_{CPD} in this mode and then determine the work function (Fig. S8 and S9), surface potentials and local charge distributions at the surface of scanned samples. For a thick region in CIPS, e.g. ~30 nm in Fig. 3d (also see Fig. S10a), the surface potential will increase as shown in Fig. 3e. Surface potential of CIPS nanoflakes can be quantitatively determined to be ~ 0.2 V higher than one of the silicon substrate, indicating that a lower charge density at the surface of CIPS nanoflakes. By heating the samples from 298 K to 318 K, the corresponding KPFM image are obtained and shown in Fig. 3f, and the surface potential quickly increases from −0.64 V to −0.51 V. It suggests that CIPS ultrathin flakes remain pyroelectric down to a few nanometers. Temperature-dependent surface potential was observed even for bilayer flake as shown in Fig. 3g-i (the thickness about 1.8 nm as shown in Fig. S10b), which is the thinnest CIPS crystal calculated to have spontaneous polarization and stable pyroelectric phase [28].

Based on the above results of the pyroelectric-induced surface potential changes, we further focus on the temperature sensitivity of pyroelectric CIPS nanoflakes. In Fig. 4, the temperature-dependent surface potential are investigated by heating the samples from 298 K to 318 K with interval of 5 K. Fig. 4d–h show the temperature dependent surface potential changes of few-layered CIPS crystal (the thickness ~30 nm as shown in Fig. S7) from −0.639 V (298 K), −0.598 V (303 K), −0.565 V (308 K), −0.537 V (313 K), to −0.519 V (318 K) with the surface potential change ΔV about ~6 mV/K. By heating the CIPS nanoflakes, the spontaneous polarization will be weakened since the Cu, In and P_2S_6 electric dipoles vibrations are within bigger spread angle due to the higher hopping motions. As a result, the whole magnitude of the spontaneous polarization is decreased, and less charges will be attracted on the surfaces. Therefore, the elevation of surface potential can be observed with a rise of temperature in Fig. 3 and Fig. 4. On the contrary, if the CIPS flake is cooled instead of heated, the spontaneous polarization evolution leads to the increase of attracted charges on the surfaces. The corresponding KPFM images are shown in Fig. S12, and the magnitude of the potential fleetly decreased from −0.513 mV to −0.644 mV. Based on the temperature-dependent surface potential changes, we could quantify the pyroelectric charge displacement and the pyroelectric coefficient, after clarifying the relationship between the charge displacement and surface potential (the details in the supporting information, Eq. S1-S3). In Fig. 3 and Fig. 4 ΔV is ~130 mV with the thickness ~30 nm and ~15 mV with the thickness ~2 nm by using $\Delta T = 20$ K. Reported works have investigated the fitted and experimental temperature dependence of CIPS dielectric permittivity, with the highest dielectric constant $\varepsilon_{pyro} = 380$ [22,29]. Therefore, according to the formulas shown as Eq. S1–3, the pyroelectric coefficient p_{CIPS} can be obtained up to ~735 μC/m^2/K, with the temperature increase, as shown in Fig. 4i.

Conductive AFM (C-AFM, sub-nA up to μA) and tunneling AFM (TUNA, sub-pA up to nA), as powerful techniques for nano-current characterizations (Fig. 5a–b) [38–40], are employed to monitor the pyroelectric current generated on CIPS by changing the temperature. An AFM conductive probe with Peakforce TUNA was used for the measurement. By heating the samples from 298 K to 318 K, the TUNA current from 30 nm CIPS flake is ~ −8pA as shown in Fig. 5d. The flow of electrons is away from the sample so the current by warming is negative in Fig. S14. On the other way, cooling the CIPS flake will enhance the polarization of CIPS and increase the charge density on the surfaces, then the positive current flows towards the sample (~9 pA in Fig. 5e). These results evidence the pyroelectricity in 2D layers of CIPS, making it a promising energy-harvesting element in vdW heterostructure. We then fabricated the CIPS based vdW devices via stacking exfoliating the CIPS flakes (20 nm) on to a Si substrate with the electrodes on the top. Fig. 5f shows the schematic of the setup and Fig. 5g represents the AFM height profile (details in Experiment Method). Generally, the pyroelectric current I of CIPS/Si vdW devices could be described as $I = p_{CIPS}A(dT/dt)$, where p_{CIPS} is the pyroelectric coefficient of the CIPS nanoflakes, A is the electrode area, (dT/dt) is the rate of the changing temperature. Therefore, the pyroelectric currents of CIPS/Si vdW device are directly proportional to the rate of the changing temperature. Fig. 5h–j shows the cyclic changes in temperature of the CIPS pyroelectric device and the corresponding *I-t* curve. A negative current pulse (about 100 pA) was observed when the temperature was increased from 298 to 308 K. After reversely cooling the CIPS from 308 to 298 K, the obtained opposite current signals indicate that the measured signals were generated by the fabricated CIPS device as a vdW pyroelectric nanogenerator. If one increases the ramping rate of the temperature, the output current also increased up to ~350 pA (Figs. 5h–5j). Furthermore, as shown in Fig. 5k, we noticed that its performance relies on the electrode size, which are discussed in Fig. S16.

4. Conclusion

In this work, we systematically studied the pyroelectricity in ultrathin CIPS. The phase transition of CIPS was first investigated via thermal evolution of the CIPS Raman spectra, indicating a transition temperature of around 320 K. Through the temperature dependent surface potential and pyroelectric current measurement, we found that, CIPS 2D nanoflakes, even the bilayer CIPS with ~2 nm thickness could generate temporary pyroelectric surface charge induced by slight atom position modifications and the polarization changes with heating or cooling. Taking advantage of pyroelectrical charges, it is the first time that ultrathin CIPS based pyroelectric nanogenerator were demonstrated based on CIPS nanoflakes for harvesting heat energy into pyroelectric currents at the room temperature. These results greatly enrich the self-powered functionalities of 2D ferroelectric materials and opens new possibilities for thermal nanosensors and ultrathin pyroelectric devices.

Acknowledgements

This work was supported by the National Research Foundation Singapore under NRF award number NRF-RF2013-08, Tier 2 MOE2017-T2-2-136, Tier 2 MOE2016-T2-2-153, MOE2015-T2-2-007, Tier 1 RG7/18, Tier 1 RG4/17. X.F.L thanks the support from the Ministry of Science and Technology (2017YFA0205004 and 2016YFA0200700), National Natural Science Foundation of China (21673054 and 11874130), Natural Science Foundation of Beijing Municipality (4182076 and 4184109).

Appendix A. Supporting information

Supplementary data associated with this article can be found in the online version at doi:10.1016/j.nanoen.2019.01.085.

References

[1] C.H. Ahn, K.M. Rabe, J.M. Triscone, Science 303 (2004) 488–491.
[2] Y. Yang, W.X. Guo, K.C. Pradel, G. Zhu, Y.S. Zhou, Y. Zhang, Y.F. Hu, L. Lin, Z.L. Wang, Nano Lett. 12 (2012) 2833–2838.
[3] Y. Yang, Y.S. Zhou, J.M. Wu, Z.L. Wang, ACS Nano 6 (2012) 8456–8461.
[4] P. Gunter, J. Appl. Phys. 48 (1977) 3475–3477.
[5] N. Ma, Y. Yang, Nano Energy 40 (2017) 352–359.
[6] K. Song, N. Ma, Y. Yang, Adv. Mater. Technol. 2 (2017) 1700221.
[7] N. Ma, K. Zhang, Y. Yang, Adv. Mater. 29 (2017) 1703694.
[8] K.W. Zhang, S.H. Wang, Y. Yang, Adv. Energy Mater. 7 (2017) 1601852.
[9] K.W. Zhang, Z.L. Wang, Y. Yang, ACS Nano 10 (2016) 10331–10338.
[10] J.F. Scott, Science 315 (2007) 954–959.
[11] C.A.P. Dearaujo, J.D. Cuchiaro, L.D. Mcmillan, M.C. Scott, J.F. Scott, Nature 374 (1995) 627–629.
[12] V. Garcia, M. Bibes, Nat. Commun. 5 (2014) 4289.
[13] J.H. Lee, K.Y. Lee, M.K. Gupta, T.Y. Kim, D.Y. Lee, J. Oh, C. Ryu, W.J. Yoo, C.Y. Kang, S.J. Yoon, J.B. Yoo, S.W. Kim, Adv. Mater. 26 (2014) 765–769.
[14] Z.N. Wang, R.M. Yu, C.F. Pan, Z.L. Li, J. Yang, F. Yi, Z.L. Wang, Nat. Commun. 6 (2015) 8401.
[15] S.H. Wang, Z.L. Wang, Y. Yang, Adv. Mater. 28 (2016) 2881–2887.
[16] X. Wang, Z.L. Wang, Y. Yang, Nano Energy 26 (2016) 164–171.
[17] Z.N. Wang, R.M. Yu, X.F. Wang, W.Z. Wu, Z.L. Wang, Adv. Mater. 28 (2016) 6880–6886.
[18] X. Li, M. Chen, R. Yu, T. Zhang, D. Song, R. Liang, Q. Zhang, S. Cheng, L. Dong, A. Pan, Z.L. Wang, J. Zhu, C. Pan, Adv. Mater. 27 (2015) 4447–4453.
[19] X.Y. Li, R.R. Liang, J. Tao, Z.C. Peng, Q.M. Xu, X. Han, X.D. Wang, C.F. Wang, J. Zhu, C.F. Pan, Z.L. Wang, ACS Nano 11 (2017) 3883–3889.
[20] H.M. Yang, W.L. Liu, Y. Xi, M.H. Lai, H.Y. Guo, G.L. Liu, M.F. Wang, T. Li, X. Ji, X.G. Li, Nano Energy 47 (2018) 539–546.
[21] M.H. Lai, L. Cheng, Y. Xi, Y.H. Wu, C.G. Hu, H.Y. Guo, B.L. Du, G.L. Liu, Q.P. Liu, R.C. Liu, J. Phys. D Appl. Phys. 51 (2018) 015303.
[22] J. Banys, J. Macutkevic, V. Samulionis, A. Brilingas, Y. Vysochanskii, Phase Transit. 77 (2004) 345–358.
[23] V.B. Cajipe, J. Ravez, V. Maisonneuve, A. Simon, C. Payen, R. Von der Muhll, J.E. Fischer, Ferroelectrics 185 (1996) 135–138.
[24] V. Maisonneuve, V.B. Cajipe, A. Simon, R. VonDerMuhll, J. Ravez, Phys. Rev. B 56 (1997) 10860–10868.
[25] V. Maisonneuve, J.M. Reau, M. Dong, V.B. Cajipe, C. Payen, J. Ravez, Ferroelectrics 196 (1997) 577–580.
[26] P. Colombet, A. Leblanc, M. Danot, J. Rouxel, J. Solid State Chem. 41 (1982)

174–184.
[27] A. Vanderlee, F. Boucher, M. Evain, R. Brec, Z. Krist. 203 (1993) 247–264.
[28] F.C. Liu, L. You, K.L. Seyler, X.B. Li, P. Yu, J.H. Lin, X.W. Wang, J.D. Zhou, H. Wang, H.Y. He, S.T. Pantelides, W. Zhou, P. Sharma, X.D. Xu, P.M. Ajayan, J.L. Wang, Z. Liu, Nat. Commun. 7 (2016) 12357.
[29] A. Belianinov, Q. He, A. Dziaugys, P. Maksymovych, E. Eliseev, A. Borisevich, A. Morozovska, J. Banys, Y. Vysochanskii, S.V. Kalinin, Nano Lett. 15 (2015) 3808–3814.
[30] A.V. Ievlev, M.A. Susner, M.A. McGuire, P. Maksymovych, S.V. Kalinin, ACS Nano 9 (2015) 12442–12450.
[31] V. Maisonneuve, M. Evain, C. Payen, V.B. Cajipe, P. Molinie, J. Alloy. Compd. 218 (1995) 157–164.
[32] A. Simon, J. Ravez, V. Maisonneuve, C. Payen, V.B. Cajipe, Chem. Mater. 6 (1994) 1575–1580.
[33] Y.M. Vysochanskii, V.A. Stephanovich, A.A. Molnar, V.B. Cajipe, X. Bourdon, Phys. Rev. B 58 (1998) 9119–9124.
[34] Y.S. Zhou, Y. Liu, G. Zhu, Z.H. Lin, C.F. Pan, Q.S. Jing, Z.L. Wang, Nano Lett. 13 (2013) 2771–2776.
[35] X.W. Wang, X.X. He, H.F. Zhu, L.F. Sun, W. Fu, X.L. Wang, L.C. Hoong, H. Wang, Q.S. Zeng, W. Zhao, J. Wei, Z. Jin, Z.X. Shen, J. Liu, T. Zhang, Z. Liu, Sci. Adv. 2 (2016) e1600209.
[36] W. Melitz, J. Shen, A.C. Kummel, S. Lee, Surf. Sci. Rep. 66 (2011) 1–27.
[37] H. Sun, H.B. Chu, J.Y. Wang, L. Ding, Y. Li, Appl. Phys. Lett. 96 (2010) 602.
[38] M. Dante, J. Peet, T.Q. Nguyen, J. Phys. Chem. C 112 (2008) 7241–7249.
[39] M. Armand, J.M. Tarascon, Nature 451 (2008) 652–657.
[40] W. Chen, Y.Z. Wu, Y.F. Yue, J. Liu, W.J. Zhang, X.D. Yang, H. Chen, E.B. Bi, I. Ashraful, M. Gratzel, L.Y. Han, Science 350 (2015) 944–948.

Dr. Lin Niu received her Ph.D. degree in 2011 at the National Center for Nanoscience and Technology (NCNST), China. She joined the school of materials science & engineering (MSE) of Nanyang Technological University (NTU), Singapore, as a postdoctoral fellow since 2015. Her research interests mainly focuses on the design and controlled synthesis of functional 2D materials and their applications in high-performance optoelectronics device, thermal nanosensor and energy conversion.

Dr. Fucai Liu is a full professor at University of Electronic Science and Technology China. He received his Ph.D. degree and B.Sc. degree from Nankai University China. After graduation, he worked as postdoc in Tohoku University Japan, Nanyang Technological University Singapore. In 2017 he was selected into the Thousand Talents program for Young Researchers. His main research interested include optical, ferroelectric and magnetic properties study of low dimensional system.

Dr. Qingsheng Zeng received his B.S. degree in Material Physics from Beijing Normal University in 2006, and obtained his Ph.D. degree in Nanoelectronics from Peking University in 2012. He is now working as a research fellow at Nanyang Technological University. His current research interests focus on the synthesis of low dimensional materials and their electronic, optoelectronic applications.

Xiaoyang Zhu received her B.S. degree in 2004 and master degree in 2007 from Henan University. From 2007, she worked as a researcher at the National Center for Nanoscience and Technology (NCNST), China. Her current research mainly concentrates on characterizations of nanostructured materials by using scanning probe microscopy.

Dr. Yanlong Wang received his B.S. degree from Jilin University (China) in 2011 and Ph.D. degree from Nanyang Technological University (Singapore) in 2016. After spending one year as a research staff at Nanyang Technological University, he joined Dalian Institute of Chemical Physics as a researcher in 2017. His research interests include 2D materials and optical thin films with functional properties.

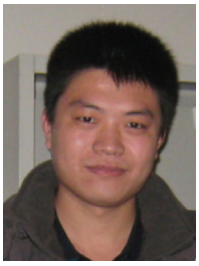

Dr. Peng Yu is an associate Professor of “100 Top Talents Program” in Sun Yat-sen University. He received his B.E. from University of Jinan in 2008 and Ph.D. from University of Chinese Academy of Science in 2013. From 2014–2018, he was a research fellow at Nanyang Technological University in the research group of Professor Zheng Liu. He joined Sun Yat-sen University in Sep. 2018 and his research interests focus on nonlinear optical materials, high-performance electronic devices and optoelectronic devices.

Jia Shi received her B.Sc. degree from Beijing University of Chemcial Techonology in 2014. She is studying at the National Center of Nanoscience and Technology for her Ph.D. degree. Her main research interests include nonlinear optics in 2D materials and quasi-particles dynamics in heterostructures.

Dr. Junhao Lin obtained Ph.D. degree of Physics from Vanderbilt University, USA, in 2015. He had his postdoctoral work as a JSPS fellow in AIST, Japan from 2015. He has been selected for the 14th thousand talent young researcher program and is now an associate professor in Southern University of Science and Technology (SuSTech). His main research direction includes analysis of complex defect structures in novel layered materials, real time in-situ observation of the dynamical processes in structural transition of materials under various environmental stimulations, and the phonon behavior of 2D materials as probed by monochromatic valence electron energy loss spectroscopy.

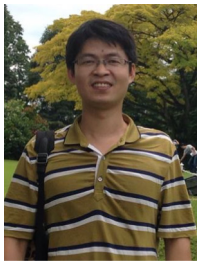

Mr. Jiadong Zhou was born in Anhui, China in 1985. He received his B.Sc. (2009) in Material Chemistry from Shaanxi University of Science & Technology and got the Master (2013) in Materials Engineering from Shanghai Institute of Ceramics, Chinese Academy of Sciences (SICCAS), under the guidance of Professor Yanfeng Gao. He completed his Ph.D. (2018) in Material Science under the guidance of Professor Zheng Liu in Nanyang Technological University. His researches are focusing on the synthesis, properties and applications of 2D materials.

Dr. Fu Qundong obtained his bachelor degree from Nankai University in 2013 and Ph.D. degree from Nanyang Technological University in 2018. He is currently working on the synthesis of novel two-dimensional materials and their electronic and optoelectronic applications.

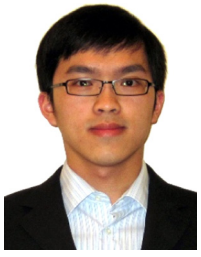

Dr. Wu Zhou received his B.Sc. degree from Tsinghua University in 2006 and Ph.D. degree from Lehigh University in 2010. After graduation, he worked as postdoc and Staff Scientist in Oak Ridge National Laboratory. In 2013 he was selected into the Thousand Talents program for Young Researchers. He joined the “100-Talents” Program of the Chinese Academy of Sciences (CAS) in 2016 and became a Professor at the school of physical sciences, University of Chinese Academy of Sciences since then. His research group mainly focuses on high resolution electron microscopy, two-dimensional quantum materials, Nano-materials for energy applications.

Dr. Ting Yu is a professor in the School of Physical and Mathematical Sciences at the Nanyang Technological University (Singapore). He received his B.Sc. degree from the Jilin University (China) in 1999 and his Ph.D. degree from the National University of Singapore in 2003. His current research focuses on low-dimensional, especially 2D, materials, and investigation of their optical, optoelectrical, and electrochemical properties for developing novel electronics, optoelectronics, and energy conversion/storage devices.

Dr. Xinfeng Liu is a professor at the National Center for Nanoscience and Technology (NCNST), China. He received his Ph.D. in 2011 at NCNST. Then he joined School of Physical and Mathematical Sciences (SPMS) of Nanyang Technological University (NTU), Singapore, as a post-doctoral fellow. He joined the “100-Talents” Program of the Chinese Academy of Sciences (CAS) in 2015 and became a Professor of NCNST since then. His research group mainly focuses on light–matter interaction and ultrafast spectroscopy at micro-to-nanometer scale.

Dr. Zheng Liu was born in Hubei, China in 1983. He received his B.Sc. (2005) and Ph.D. (2010) in Physics from National Center for Nanoscience and Technology (NCNST), China, under the guidance of Professor Lianfeng Sun. He is Associate Professor at Nanyang Technological University. His research focus on the growth, characterizations and performance of large-scale and high-quality novel low-dimensional crystals, including, hexagonal boron nitride, metal dichalcogenides and their hybridized architectures, as well as their applications on high-performance electronics, optical devices and energy conversion and storage.